European Journal of Mechanics / A Solids 72 (2018) 88–96

Contents lists available at ScienceDirect

European Journal of Mechanics / A Solids

journal homepage: www.elsevier.com/locate/ejmsol

Exact solution for the mode III stress fields ahead of cracks initiated at sharp notch tips

Marco Salviato[a,*], Michele Zappalorto[b], Lucio Maragoni[b]

[a] William E. Boeing Department of Aeronautics & Astronautics, University of Washington, 311D Guggenheim Hall, Seattle, WA 98195-2400, United States
[b] University of Padova, Department of Management and Engineering, Stradella San Nicola 3, 36100, Vicenza Italy

ARTICLE INFO

Keywords:
Antiplane shear
Torsion
Crack
Notch
Stress distribution

ABSTRACT

In this work, the exact solution for the stress fields ahead of cracks initiated at sharp notch tips under antiplane shear and torsion loadings is derived in close form, leveraging conformal mapping and the complex potential method for antiplane elasticity.

Based on the stress field distributions, relevant expressions for the mode III crack stress intensity factors are derived and their accuracy is discussed in detail taking advantage of a bulk of results from FE analyses.

1. Introduction

Stress concentrators, such as notches and holes, are unavoidably present in mechanical components, leading to cracking phenomena both under static and fatigue loadings.

Explicitly or implicitly, local approaches to the static and fatigue design of mechanical components are based on the local stress fields close to notch tips (see among the others, Yosibash and Mittelman, 2016, and references reported therein) thus justifying the large attention paid over the decades in the literature to the study of this problem (see, just to mention a few: Inglis, 1913, Neuber, 1958, Creager and Paris, 1967, Kullmer, 1992, Lazzarin and Tovo, 1996, Zappalorto et al., 2010, Zappalorto and Lazzarin, 2011, Feriani et al., 2011, Felger and Becker, 2017, Zappalorto and Maragoni, 2018).

When dealing with cyclic loadings, notch tip stresses are thought of as controlling the fatigue life spent to initiate short cracks fully immersed in the stress field of the un-cracked (notched) component. For some relevant applications, such as the design against fatigue of steel and aluminum welded joints, the initiation life is the major part of the entire life of the component and fatigue life predictions can be simply based on Williams' asymptotic stress field distribution around the un-cracked weld toe or root region (Livieri and Lazzarin, 2005).

In the case of notched (unwelded) components, instead, the ratio between the number of cycles to crack initiation and those to failure strictly depends on the notch tip radius. For large radii, the initiation phase is predominant, whereas, when the notch tip radius is very small, the propagation phase becomes more and more important (Lazzarin et al., 1997). Similar arguments can be used also in the case of manufacturing defects (see, among the others, Atzori et., 2003, Carraro et al., 2015, Maragoni et al., 2016). In all these cases, the propagation phase cannot be neglected, and should be assessed taking advantage of the integration of the Paris' fatigue curve. To this end, the knowledge of the crack stress intensity factor is essential and many authors devoted great efforts to determine K values for cracks emanating from notches.

The literature on this topic is so broad that a comprehensive review is far from easy and, especially, is out of the specific aim of the present paper. In the following, only some examples will be discussed, without the ambition to be thorough. Worth of being mentioned is the paper by Bowie (1956), who gave the solutions for a circular hole with a single edge crack and a pair of symmetrical edge cracks in a plate under tension, whilst Tweed and Rooke (1973) used the Mellin transform technique to study the case of a branching crack emanating from a circular hole under biaxial tension. The analysis was also extended to elliptical holes by Newman (1971) and Murakami (1978) who studied the tension problem for an elliptical hole with symmetrical edge cracks, and Isida and Nakamura (1980) who analysed a slant crack emanating from an elliptical hole under far applied uniaxial tension and shear.

The problem of cracks initiating at edge rounded notches was also comprehensively debated, amongst the others, by Lukas and Klesnil (1978), Bandyopadhyay and Deysarker (1981), Shijve (1982), Kujawskii (1991) and Xu et al. (1997) whereas cracks from sharp notches or holes were studied by Neal (1970), Muki and Westman (1974), Hasebe and Ishida (1978) and Hasebe and Ueda (1980), just to mention a few.

Despite such an intense scrutiny carried out in the previous century, this topic is still attracting the interests of researchers, as documented

* Corresponding author.
E-mail addresses: salviato@aa.washington.edu (M. Salviato), michele.zappalorto@unipd.it (M. Zappalorto).

https://doi.org/10.1016/j.euromechsol.2018.04.014
Received 26 December 2017; Received in revised form 12 April 2018; Accepted 17 April 2018
Available online 23 April 2018
0997-7538/

by some works published in the more recent literature related to cracks emanating from rounded notches (see for example Jones and Peng, 2002, Xiangqiao Yan, 2004, 2005; 2006; The et al., 2006; Abdelmoula et al., 2007; Weiβgraeber et al., 2016a,b) as well as from singular points (Philipps et al., 2008; Iida and Hasebe, 2016; Weiβgraeber et al., 2016a,b).

However, in the best of the authors' knowledge, the analytical study of the whole stress fields ahead of cracks nucleated at the tip of notches, accounting for the combined effect of the crack tip singularity and notch stresses, has received far less attention so far. Within this context, worth of mention is the work by Hasebe and Ishida (1978) who provided the solution for a crack originating from a triangular notch on a rim of a semi-infinite plate, and the paper by Hasebe and Ueda (1980) who studied the stress field of a crack originating from a square hole corner. In both cases, the proposed solution is exact but very complicated, and a simple expression for the stress field was not given in an explicit form.

The aim of the present paper is to partially fill this gap providing an exact yet simple stress field solution for a crack emanating from a pointed V notch in a plate subjected to antiplane shear loading and in a solid bar under torsion.

To this end, the conformal mapping technique is used in combination with a recent approach proposed by the authors (Salviato and Zappalorto, 2016), according to which the exact mode III stress field can be determined using the complex potential approach applied to the first derivative of the conformal mapping function.

Two relevant cases are addressed and solved separately:

- the mode III problem of a finite crack nucleating from a deep (mathematically infinite) pointed V notch in a body with a finite ligament;
- the mode III problem of a finite crack nucleating from a finite depth pointed V notch in a body with an infinite ligament.

Relevant, exact, expressions for the mode III crack stress intensity factors are also provided.

The accuracy of the proposed solutions is discussed, taking advantage of the comparison with the results from FE analyses carried out on elastic bodies subjected to antiplane shear and torsion loadings, showing a very satisfactory agreement also in the case of fully finite bodies.

2. Preliminary remarks

Consider a body made of a homogenous and isotropic material obeying the theory of linear elastic deformations. Further, consider the Cartesian reference system (x,y,z) represented in Fig. 1 and suppose that the body is loaded by a remote shear stress τ_∞ resulting only in displacements w in the z direction, normal to the plane of the notch characterized by the x and y axes (Fig. 1a).

Let us consider a notch profile and a conformal map $z = z(\xi)$ with

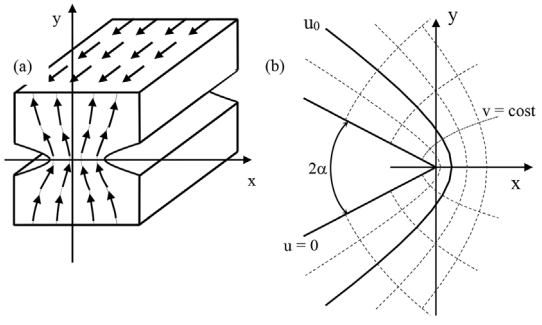

Fig. 1. (a) Notched body under longitudinal shear; (b) Typical conformal mapping describing the notch. The boundary is defined by the condition $u = u_0$.

$\xi = u + iv$ and $z = x + iy$ such that the notch profile is described by the condition $u(x, y) = u_0$ (Fig. 1b). The constant u_0 is taken as a positive number, so that the domain of integration belongs to the right half plane of the (u,v) space.

In the foregoing conditions, the out-of-plane displacement component w is harmonic (Timoshenko and Goodier, 1970) whereas the other components are equal to zero. Thanks to the properties of conformal mapping, the harmonicity of the displacement function $\omega(u, v) = w\{x(u, v), y(u, v)\}$ with respect to the curvilinear coordinates u and v is left intact (Greenberg, 2001; Salviato and Zappalorto, 2016):

$$\frac{\partial^2\omega}{\partial u^2} + \frac{\partial^2\omega}{\partial v^2} = 0 \tag{1}$$

The foregoing equation can be solved assuming separation of variables in curvilinear coordinates:

$$\omega = f(u)g(v) \tag{2}$$

Substituting Eq. (2) into (1) leads to:

$$f''(u)g(v) + f(u)g''(v) = 0 \tag{3}$$

or, equivalently:

$$\frac{f''(u)}{f(u)} = \frac{g''(v)}{g(v)} = \lambda^2 \tag{4}$$

where λ is real a constant. Accordingly, the governing PDE can be simplified into two ODE in the variables u, v:

$$f''(u) - \lambda^2 f(u) = 0 \quad g''(v) + \lambda^2 g(v) = 0 \tag{5}$$

With the aim to introduce the relevant boundary conditions, the following expressions for strains and stresses in curvilinear coordinate are useful (Sokolnikoff, 1983):

$$\gamma_{iz} = \frac{1}{h_i}\frac{\partial\omega}{\partial\alpha_i} \quad \tau_{iz} = \frac{G}{h_i}\frac{\partial\omega}{\partial\alpha_i} \tag{6}$$

where G is the elastic modulus in shear and h_i is the factor of distortion (Neuber, 1958).

As, in general, $h_i \neq 0$, the *Dirichlet conditions* in terms of stresses result in *Von Neuman* conditions on ω.

The problem is then defined by the following system of equations:

$$\begin{cases} g''(v) + \lambda^2 g(v) = 0 \\ f''(u) - \lambda^2 f(u) = 0 \\ f'(u_0) = 0 \\ \frac{|f'(u)|}{h_u} < \infty \quad for \quad u, v \to \infty \\ \frac{|g'(v)|}{h_v} < \infty \quad for \quad u, v \to \infty \end{cases} \tag{7a–e}$$

where Eq. (7c) is the free-of-stress condition along the notch edge, whereas Eq. (7d,e) express the condition for bounded stresses far away the notch tip.

The case $\lambda^2 \neq 0$ can be disregarded as it provides trivial solutions only. Differently, under the condition $\lambda^2 = 0$, the general solution:

$$\omega(u, v) = (A + Bu)(C + Dv) \tag{8}$$

can be further simplified into Eq. (9) to account for boundary conditions:

$$\omega(u, v) = C_1 + C_2 v \tag{9}$$

where C_1 represents a rigid translation which does not contribute to the strain field and can be ignored.

Introducing Eq. (9) into the definition of stresses and invoking Cauchy-Riemann conditions, one gets the following expressions:

$$\tau_{zx} = \varsigma\frac{\partial v}{\partial x} \quad \tau_{zy} = \varsigma\frac{\partial u}{\partial x} \tag{10}$$

$\varsigma = GC_2$ being a constant to determine. It is worth noting that, as $\xi' = d$

$\xi(z)/dz = \partial u/\partial x + i\partial v/\partial x$, shear stresses represent the real and imaginary parts of the first derivative of the conformal map used to describe the notch profile, $\xi = \xi(z)$:

$$\tau_{zy} + i\tau_{zx} = \varsigma\frac{d\xi(z)}{dz} \tag{11}$$

This result provides an explicit link between the domain geometry and the stress field. Once a suitable conformal map is found, the problem of finding the generated stress field can be solved directly, except for one constant ς, which can be found analytically for finite notches and cracks or it can be generally computed by FE analyses.

Sometimes it is convenient to describe the notch profile by the condition $v(x, y) = v_0$. This is the case, for instance, in which the conformal map used to describe the domain is constructed by the *Schwarz-Christoffel* transformation.

The derivation of the stress field is similar to that given in the foregoing section, provided that the following system of ODE is considered:

$$\begin{cases} g''(v) - \lambda^2 g(v) = 0 \\ f''(u) + \lambda^2 f(u) = 0 \\ g'(v_0) = 0 \\ \frac{|g'(v)|}{h_v} < \infty \quad for \quad u, v \to \infty \\ \frac{|f'(u)|}{h_u} < \infty \quad for \quad u, v \to \infty \end{cases} \tag{12a–e}$$

which results in:

$$\tau_{zx} = \varsigma\frac{\partial u}{\partial x} \quad \tau_{zy} = -\varsigma\frac{\partial v}{\partial x} \tag{13a-b}$$

or equivalently:

$$\tau_{zx} - i\tau_{zy} = \varsigma\frac{d\xi(z)}{dz} \tag{14}$$

ς being a constant to determine.

3. Stress fields for a crack initiated at the tip of a deep pointed V notch in a solid with finite net section

3.1. Complete solution for the antiplane shear problem

Consider the following mapping function:

$$z = (\xi^2 + a^{2/q})^{q/2} \tag{15}$$

where z = x + iy, $\xi = u + iv$, a > 0 and 1 < q < 2. The case $u = u_0 = 0$ represents a finite crack initiated at the tip of a deep pointed V notch (see Fig. 2) where a > 0 represents the crack length and q is linked to the notch opening angle according to the following expression:

$$q = \frac{2\pi - 2\alpha}{\pi} \tag{16}$$

Inverting Eq. (15) gives:

$$\xi = \sqrt{z^{2/q} - a^{2/q}} \tag{17}$$

so that:

$$\frac{\partial\xi}{\partial z} = \frac{z^{\frac{2}{q}-1}}{q\sqrt{z^{2/q} - a^{2/q}}} \tag{18}$$

Substituting Eq. (18) into Eq. (11) gives:

$$\tau_{zy} + i\tau_{zx} = \varsigma\frac{z^{\frac{2}{q}-1}}{q\sqrt{z^{2/q} - a^{2/q}}} \tag{19}$$

Eq. (19) can be re-written as it follows:

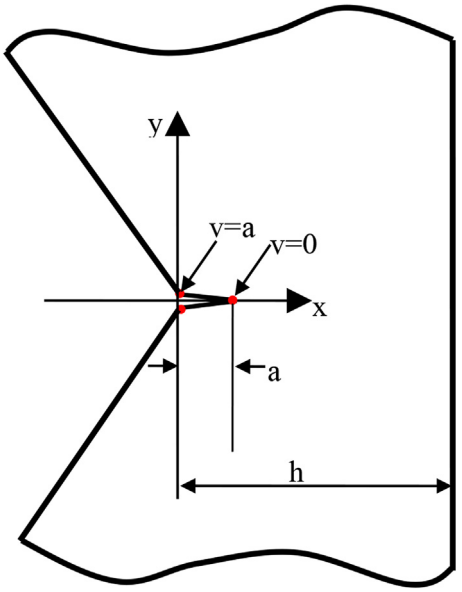

Fig. 2. Schematic of the conformal mapping given by Eq. (15).

$$\tau_{zy} + i\tau_{zx} = \varsigma\frac{r^{\frac{2}{q}-1}e^{i\left\{\left(\frac{2}{q}-1\right)\theta - \frac{\psi}{2}\right\}}}{q\sqrt{R}} \tag{20}$$

Where:

$$R = \left(r^{4/q} + a^{4/q} - 2a^{2/q}r^{2/q}\cos\frac{2\theta}{q}\right)^{1/2}$$
$$\psi = Ph\left\{\cos 2\,\theta/q - \left(\frac{a}{r}\right)^{2/q} + i\sin 2\,\theta/q\right\} \tag{21a-b}$$

Accordingly:

$$\begin{Bmatrix}\tau_{zx}\\ \tau_{zy}\end{Bmatrix} = \varsigma\frac{r^{\frac{2}{q}-1}}{q\sqrt{R}}\begin{Bmatrix}\sin\left[\left(\frac{2}{q}-1\right)\theta - \frac{\psi}{2}\right]\\ \cos\left[\left(\frac{2}{q}-1\right)\theta - \frac{\psi}{2}\right]\end{Bmatrix} \tag{22}$$

Eq. (22) gives the closed form expression for stresses as a function of the unknown constant ζ.

3.2. Analytical solution for the stress intensity factor for antiplane shear loadings

With the aim to determine an analytical solution for the Stress Intensity Factor (SIF), K_{III}, Eq. (19) can be evaluated along the crack bisector line, thus giving:

$$\tau_{zy} = \varsigma\frac{x^{\frac{2}{q}-1}}{q\sqrt{x^{2/q} - a^{2/q}}} \tag{23}$$

Close to the crack tip $x \approx a + \varepsilon$ with ε much smaller than a, so that:

$$(a + \varepsilon)^{2/q} \cong a^{2/q} + \frac{2}{q}a^{2/q-1}\varepsilon \tag{24}$$

Substituting Eq. (24) into Eq. (23) results in the following expression, valid very close to the crack tip:

$$\tau_{zy} = \varsigma\frac{a^{\frac{1}{q}-1/2}}{\sqrt{2q\varepsilon}} \tag{25}$$

Thus:

$$K_{III} = \lim_{\varepsilon\to 0}\sqrt{2\pi\varepsilon}\cdot\tau_{zy}(y = 0) = \varsigma\sqrt{\frac{\pi}{q}}a^{\frac{1}{q}-\frac{1}{2}} \tag{26}$$

Eq. (26) provides an explicit link between the mode III SIF and the

unknown constant ζ.

In addition, the following global equilibrium condition can be imposed along the net section:

$$\int_a^h \tau_{zy} dx = \tau_{nn}(h-a) \tag{27}$$

where τ_{nn} is the nominal shear stress on the net ligament and h is the ligament width.

Substituting Eq. (23) into Eq. (27) results in:

$$\varsigma = \frac{\tau_{nn}(h-a)}{a^{1/q}\sqrt{\left(\frac{h}{a}\right)^{2/q}-1}} \tag{28}$$

Eq. (28) provides an explicit link between the nominal shear stress on the net section and the unknown constant ζ.

Substituting Eq. (28) into Eq. (26) allows the following analytical expression for the mode III SIF to be determined:

$$K_{III} = \frac{h/a-1}{\sqrt{q}\sqrt{\left(\frac{h}{a}\right)^{2/q}-1}}\tau_{nn}\sqrt{\pi a} \tag{29}$$

Eq. (29) can be re-arranged as:

$$K_{III} = Y\cdot\tau_{nn}\sqrt{\pi a} \tag{30}$$

Where:

$$Y = \frac{h/a-1}{\sqrt{q}\sqrt{\left(\frac{h}{a}\right)^{2/q}-1}} \tag{31}$$

is a dimensionless function accounting for geometry effects.

Eventually, substituting Eq. (26) into Eq. (22) gives the whole stress field as a function of the crack stress intensity factor:

$$\begin{Bmatrix}\tau_{zx}\\ \tau_{zy}\end{Bmatrix} = \frac{K_{III}}{\sqrt{q\pi}}\frac{(r/\sqrt{a})^{\frac{2}{q}-1}}{\sqrt{R}}\begin{Bmatrix}\sin\left[\left(\frac{2}{q}-1\right)\theta-\frac{\psi}{2}\right]\\ \cos\left[\left(\frac{2}{q}-1\right)\theta-\frac{\psi}{2}\right]\end{Bmatrix} \tag{32}$$

Along the notch bisector line, Eq. (32) significantly simplifies to give:

$$\tau_{zy} = \frac{K_{III}}{\sqrt{q\pi}}\frac{(x/\sqrt{a})^{\frac{2}{q}-1}}{\sqrt{x^{2/q}-a^{2/q}}} \tag{33}$$

3.3. Limiting solutions

Once the complete solution for the stress field is determined, asymptotic (limiting) solutions valid very close to or far from the crack tip can be derived, as well.

In particular, very close to the crack tip, $z \approx a + \tilde{z}$, where $\tilde{z}$ is a complex number much smaller than a, $\tilde{z} = \tilde{r}e^{i\tilde{\vartheta}}$ where $\tilde{r}$ is the radial distance from the crack tip, and $\tilde{\vartheta}$ is the polar angle of a polar system centred at the crack tip. Under these conditions, Eq. (19) can be re-written as:

$$\begin{aligned}\tau_{zy} + i\tau_{zx} &= \varsigma\frac{(a+\tilde{z})^{\frac{2}{q}-1}}{q\sqrt{(a+\tilde{z})^{2/q}-a^{2/q}}} \cong \varsigma\frac{a^{\frac{1}{q}-1/2}}{\sqrt{2q\tilde{z}}}\\ &= \varsigma\frac{a^{\frac{1}{q}-1/2}}{\sqrt{2q\tilde{r}}}\left\{\cos\frac{\tilde{\vartheta}}{2} + i\sin\frac{\tilde{\vartheta}}{2}\right\}\end{aligned} \tag{34}$$

Substituting ζ from Eq. (26) into Eq. (34) and separating the real and imaginary part gives:

$$\begin{Bmatrix}\tau_{zx}\\ \tau_{zy}\end{Bmatrix} = \frac{K_{III}}{\sqrt{2\pi\tilde{r}}}\begin{Bmatrix}\sin\frac{\tilde{\vartheta}}{2}\\ \cos\frac{\tilde{\vartheta}}{2}\end{Bmatrix} \tag{35}$$

It is worth noting that the limit solution valid very close to the crack tip, Eq. (35), where the effect of the crack singularity is predominant, perfectly matches the conventional solution from the Linear Elastic Fracture Mechanics.

Different, very far from the crack tip, where the influence of the crack tip singularity is very weak, z≫a, so that Eq. (19) simplifies to give:

$$\tau_{zy} + i\tau_{zx} = \frac{\varsigma}{q}z^{\frac{1}{q}-1} \tag{36}$$

In agreement with the solution for a pointed V-notch without a crack (see Zappalorto et al., 2010).

3.4. Extension to notches with finite depth

As already argued by Zappalorto et al. (2010) for other notched geometries, in the case of a notch with a finite depth, Eq. (32) can still be used to characterise the local stress fields close to the geometrical variation. In such a case, the value of K_{III} will be different from that given by Eq. (29).

3.5. Extension to torsion loadings

The stress fields close to the tip of a stress concentrator under torsion are identical to those under antiplane shear (Zappalorto et al., 2010). Accordingly, Eq. (35) can be extended also to the case of circumferential shafts under torsion loadings. In such a case, as suggested by Zappalorto et al. (2010), Eq. (33) can be corrected to account for the linear decreasing of the nominal stress:

$$\tau_{zy} = \frac{K_{III}}{\sqrt{q\pi}}\frac{(x/\sqrt{a})^{\frac{2}{q}-1}}{\sqrt{x^{2/q}-a^{2/q}}}\left(1-\frac{x-a}{P}\right) \tag{37}$$

where P is the radius of the net section of the shaft.

4. Finite crack initiated at the tip of a finite pointed V-NOTCH in a plate with a very large ligament

Consider the mapping shown in Fig. 3 describing a finite pointed V-notch of depth b weakened by a crack, of length a, emanating from the notch tip. Leveraging a Schwarz–Christoffel transformation, the first derivative of the mapping can be calculated as follows:

$$Z'(\xi) = A\frac{\xi}{(\xi^2-f^2)^{\beta/\pi}(\xi^2-g^2)^{1/2-\beta/\pi}} \tag{38}$$

where A is a complex constant and f and g are real quantities such that f > g > 1. Now,

$$\tau_{zx} + i\tau_{zy} = \varsigma\frac{d\xi}{dZ} = \varsigma[Z'(\xi)]^{-1} = \frac{\varsigma}{A}\frac{(\xi^2-f^2)^{\beta/\pi}(\xi^2-g^2)^{1/2-\beta/\pi}}{\xi} \tag{39}$$

which, considering that $\lim_{\xi\to\infty}(\tau_{zx}+i\tau_{zy}) = \varsigma/A = \tau_\infty$, can be related to the remote stress as follows:

$$\tau_{zx} + i\tau_{zy} = \tau_\infty\frac{(\xi^2-f^2)^{\beta/\pi}(\xi^2-g^2)^{1/2-\beta/\pi}}{\xi} \tag{40}$$

The foregoing equation provides the Cartesian stresses as a function of the curvilinear coordinates used to describe the domain of interest. The equation can be rewritten in Cartesian coordinates provided that the mapping $\xi = \xi(Z)$ is known. However, finding such a mapping requires the integration of Eq. (38) and its inversion, an operation that is generally nontrivial. Considering that mainly the stresses close to the tip are of interest, the foregoing operation can be made relatively easy by leveraging a Taylor series expansion around the crack tip:

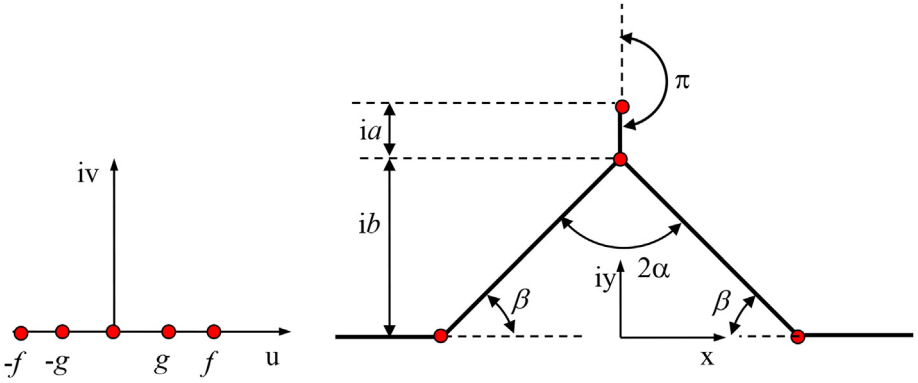

Fig. 3. Schematic of the conformal mapping given by Eq. (38).

$$\frac{Z - i(a+b)}{\xi} = \frac{i(a+b) - i(a+b)}{\xi} + \left(\frac{Z'}{\xi} - \frac{Z - i(a+b)}{\xi}\right)_{\xi\to 0} \xi + O(\xi^2) \tag{41}$$

The second term of the foregoing expression includes a 0/0 limit that, luckily, can be solved easily leveraging De l'Hospital's rule. Accordingly, Eq. (41) can be rewritten as follows:

$$\frac{Z - i(a+b)}{\xi} = \left(\frac{Z'}{\xi} - \frac{Z'}{2\xi}\right)_{\xi\to 0} \xi + \vartheta(\xi^2) \tag{42}$$

Now, introducing the transformation of coordinates:

$$z = Z - i(a+b) \tag{43}$$

the Cartesian coordinates close to the tip can be approximated as:

$$z \approx \frac{1}{2}\frac{Z'}{\xi}\bigg|_{\xi\to 0} \xi^2 \tag{44}$$

Accordingly,

$$z \approx \sqrt{\frac{2\xi}{Z'}}\bigg|_{\xi>0} Z^{1/2} \tag{45}$$

Finally, substituting (38) into (45), one gets:

$$\xi \approx \sqrt{2} f^{\beta/\pi} g^{1/2-\beta/\pi} e^{i\pi/4} \left(\frac{z}{A}\right)^{1/2} \tag{46}$$

Now, going back to the stress function and taking advantage of Eq. (46), one obtains the following expression for stress field near the crack tip (ξ→ 0):

$$\tau_{zx} + i\tau_{zy} = \frac{\tau_\infty}{\sqrt{2r}} A^{1/2} f^{\beta/\pi} g^{1/2-\beta/\pi} e^{i\pi/4-\theta/2} \tag{47}$$

where the polar transformation $z = re^{i\theta}$ was used and, it is worth mentioning, $z = re^{i\theta} \to 0$ moving towards the crack tip. Setting θ = π/2, K_{III} can then be calculated by using its definition:

$$K_{III} = \lim_{r\to 0} \sqrt{2\pi r \tau_{zx}} = \tau\infty \sqrt{A\pi} f^{\beta/\pi} g^{1/2-\beta/\pi} \tag{48}$$

Equation (48) requires the calculation of A, f and g. This can be done by integrating Eq. (38), which leads to the following expressions:

$$Z(\xi) = \int Z'(\xi) d\xi + B \tag{49}$$

$$Z(\xi) = \frac{A\pi}{2\beta + \pi}\left(\frac{1}{g^2 - f^2}\right)^{\beta/\pi} (\xi^2 - g^2)^{1/2+\beta/\pi} \chi\left(\frac{\xi^2 - g^2}{f^2 - g^2}\right) + B \tag{50}$$

where

$$\chi\left(\frac{\xi^2 - g^2}{f^2 - g^2}\right) = {}_2F_1\left[1/2 + \beta/\pi, \beta/\pi, 3/2 + \beta/\pi, \frac{\xi^2 - g^2}{f^2 - g^2}\right] \tag{51}$$

and ${}_2F_1(a, b, c, z) = \sum_{k=0}^{\infty} (a)_k (b)_k / (c)_k z^k / k!$ is the Gaussian hypergeometric function (see e.g. Yoshida, 1997; Andrews et al., 1999). Now, imposing the limit conditions Z(g) = Z(-g) and Z(0) + B = i(a + b), one gets:

$$B = ib \tag{52}$$

$$A = \frac{a(f^2 - g^2)^{\beta/\pi}(2\beta + \pi)}{\pi g^{1+2\beta/\pi} \chi[g^2/(g^2 - f^2)]} \tag{53}$$

Now, according to the mapping represented in Fig. 3, the imaginary part of $Z(\pm f)$ should be zero as the points $\pm f$ are transformed to locations that belong to the line iy = 0. This condition can be expressed by the following equation:

$$\lim_{\xi\to\pm f} IM[Z(\xi)] = b - \frac{2a \sin\beta\Gamma(1-\beta/\pi)\Gamma(3/2+\beta/\pi)(f^2 - g^2)^{1/2+\beta/\pi}}{\sqrt{\pi} g^{1+2\beta/\pi} \chi[g^2/(g^2 - f^2)]} = 0 \tag{54}$$

The foregoing equation can be used to find the relation between a/b = ρ and f and g:

$$\rho = \frac{\sqrt{\pi} g^{1+2\beta/\pi} \chi[g^2/(g^2 - f^2)]}{2\sin\beta\Gamma(1-\beta/\pi)\Gamma(3/2+\beta/\pi)(f^2 - g^2)^{1/2+\beta/\pi}} \tag{55}$$

which can be conveniently rewritten as a function of $t = g/f$ with t in [0,1]:

$$\rho = \frac{\sqrt{\pi} t^{1+2\beta/\pi} \chi[t^2/(t^2 - 1^2)]}{2\sin\beta\Gamma(1-\beta/\pi)\Gamma(3/2+\beta/\pi)(1 - t^2)^{1/2+\beta/\pi}} \tag{56}$$

Leveraging Eq. (56), the ratio between the crack length and the notch depth, ρ, can be calculated for a given t. Yet, it would be convenient to have $t = t(\rho)$. However, finding this function in closed-form is significantly cumbersome. A possible way to overcome the issue is using Asymptotic Matching. For instance, for t ~ 0 one has:

$$\rho \approx \frac{\sqrt{\pi} t^{1+2\beta/\pi}}{2\sin\beta\Gamma(1-\beta/\pi)\Gamma(3/2+\beta/\pi)} \tag{57}$$

And the small-scale asymptotic behaviour results to be:

$$t_{small} \approx \left[\frac{2\rho \sin\beta\Gamma(1-\beta/\pi)\Gamma(3/2+\beta/\pi)}{\sqrt{\pi}}\right]^{1/(1+2\beta/\pi)} \tag{58}$$

On the other hand, for ρ → ∞, t → 1.

A possible function satisfying the proper asymptotes is the following:

$$t(\rho) = \frac{t_{small}(\rho)}{\left\{1 + [t_{small}(\rho)]^{\psi(\beta)}\right\}^{1/\psi(\beta)}} \tag{59}$$

where t_{small} (ρ) is the function describing the small-scale behaviour, Eq. (58), and Ψ is a function solely of the angle β or, recalling that $\beta = (\pi - 2\alpha)/2$, the opening angle 2α. For every opening angle, this

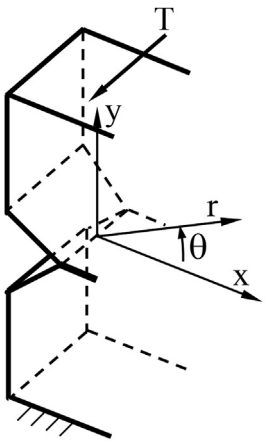

(a)

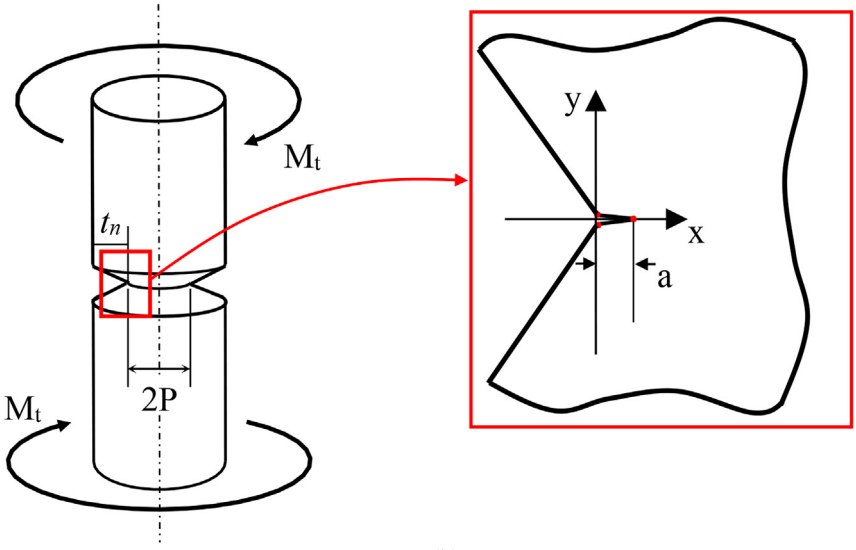

(b)

Fig. 4. Geometries used in the FE analyses. (a) Finite size plate under antiplane shear with cracks nucleating at the tip of a pointed V notch. (b) Finite size axisymmetric components under torsion with circumferential cracks nucleating at the tip of a pointed V notch.

function was determined by fitting against Eq. (56) using the Levenberg-Marquardt algorithm (Levenberg, 1944; Marquardt, 1963). The resulting expression for K_{III}, taking advantage of Eqs (39) and (40) and re-writing in terms of the opening angle 2α, is:

$$K_{III} = \frac{\tau_\infty \sqrt{2a(\pi-\alpha)}\,(1-t^2)^{(\pi-2\alpha)/4\pi}}{t^{(\pi-2\alpha)/\pi}\sqrt{\chi\left(\frac{t^2}{t^2-1}\right)}} = \tau_\infty \sqrt{\pi a}\, Y(\alpha,\rho) \tag{60}$$

$$Y(\alpha,\rho) = \frac{\sqrt{2(1-\alpha/\pi)}\,(1-t^2)^{(\pi-2\alpha)/4\pi}}{t^{(\pi-2\alpha)/\pi}\sqrt{\chi\left(\frac{t^2}{t^2-1}\right)}} \tag{61}$$

$$t(\rho) = \frac{t_{small}(\rho)}{\left\{1+[t_{small}(\rho)]^{\psi(\alpha)}\right\}^{1/\psi(\alpha)}} \tag{62}$$

$$\psi(\alpha) = 2.4772 - 0.2863\alpha \tag{63}$$

where $\chi\left(\frac{t^2}{t^2-1}\right) = {}_2F_1\left[1-\frac{\alpha}{\pi}, \frac{1}{2}-\frac{\alpha}{\pi}, 2-\frac{\alpha}{\pi}, \frac{t^2}{t^2-1}\right]$ is conveniently re-written in terms of the opening angle 2α. The difference between the foregoing expression and the analytical solution is always lower than 2%. This conclusion was made after comparing the two functions for ρ in [0, 1000] and for more than a hundred notch opening angles from 0 to π.

5. Comparison with FE results

A large bulk of finite element analyses were carried out to compare the theoretical predictions for the stress fields and the numerical results considering plate under longitudinal shear as well as solid bars under torsion.

All the FE analyses were carried out with the Ansys® 15 software package, using a very fine mesh pattern in order to get the desired degree of accuracy of the numerical results in the highly stressed region (the size of the elements close to the crack tip is about $2.5{\cdot}10^{-3}$ mm).

The stress fields under antiplane shear loadings were investigated taking advantage of the analogies existing between the in-plane electrical conduction problem and the mechanical anti-plane shear problem. Accordingly, 8 nodes elements (plane 230) were used to carry out 2D electrostatics FE analyses, using the shear moduli of the material as conductivity value and assessing the shear stresses by simply reversing

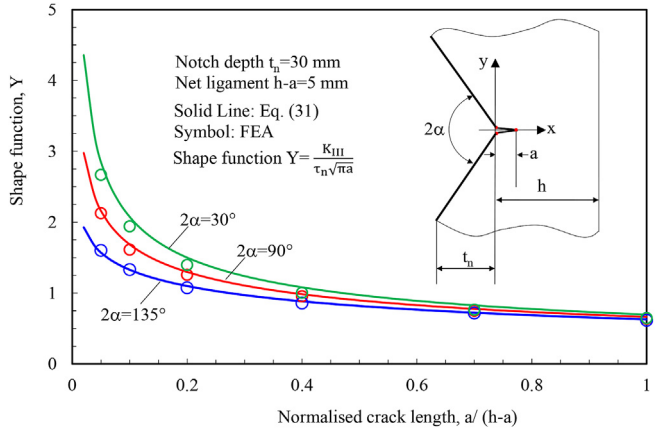

Fig. 5. Mode III shape function for cracks emanating from deep V-notches. Comparison between Eq. (31) and FE results carried out on finite plates under uniform antiplane shear loadings. Notch depth t_n = 30 mm, net ligament h-a = 5 mm. Different notch opening angles and crack lengths.

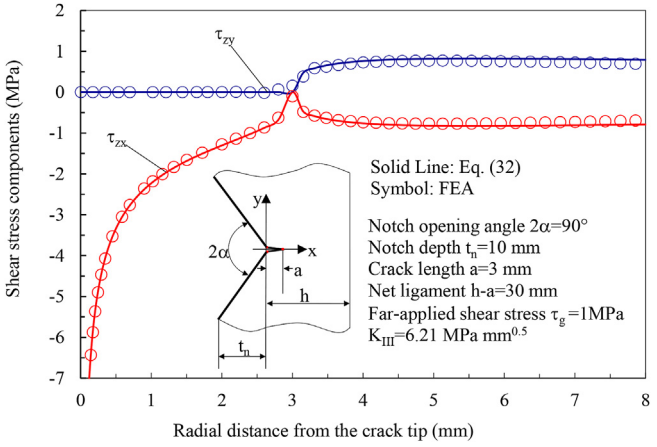

Fig. 7. Shear stress distribution along the crack and notch boundary. Comparison between Eq. (32) and FE results. Finite plate with a 3 mm long crack nucleating from a pointed V notch. Uniform antiplane shear loadings.

the sign to the values of the current densities determined. Different, the axisymmetric harmonic element (PLANE83 in ANSYS) has been used to carry out the finite element analyses under torsion.

The geometries used in the FE analyses are shown in the schematics reported in Fig. 4, while the results from the numerical analyses are compared to the theoretical predictions in Figs. 5–11.

In particular, Fig. 5 shows a comparison between the shape function assessed using Eq. (31), valid for cracks nucleated from deep V notches under uniform antiplane shear loadings, and the numerical results. The latter were obtained on plates with a net ligament equal to 5 mm weakened by a pointed V-notch with depth t = 30 mm, from which cracks of different length were thought to be nucleated. Different notch opening angles were considered, namely 2α = 30°, 90° and 135°. As evident, the agreement is very satisfactory. It is also evident that increasing the normalized crack length, the effect of the notch opening angle becomes less and less important. For a/(h-a) greater than 0.75 the difference between 2α = 30° and 2α = 135° is less than 15%.

Shear stresses evaluated on a finite plate with net ligament equal to 30 mm under antiplane shear are presented in Figs. 6–9. The plate is weakened by a 3 mm long crack nucleated from the tip of a pointed V notch with depth t = 10 mm and notch opening angle 2α = 90°. In particular, stresses were evaluated along the crack line (Fig. 6), along the crack and notch edge (Fig. 7) and along two circular paths of radius 0.3 mm and 0.9 mm centred on the crack tip (Fig. 8) and compared with the analytical predictions obtained using Eq. (32). In addition, the effect of the notch opening angle on the stress distribution is shown in Fig. 9. In all cases, the agreement between the analytical predictions and the numerical results is noteworthy.

Fig. 10, instead, shows the shear stress distribution on a solid bar

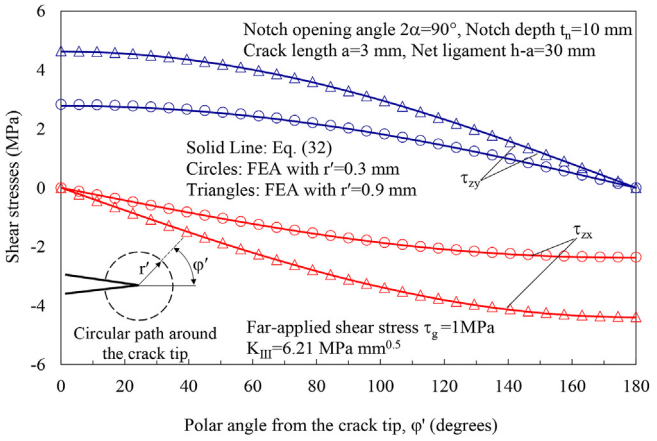

Fig. 8. Shear stress distribution along two circular paths centred on the crack tip. Comparison between Eq. (32) and FE results. Finite plate with a 3 mm long crack nucleating from a pointed V notch. Uniform antiplane shear loadings.

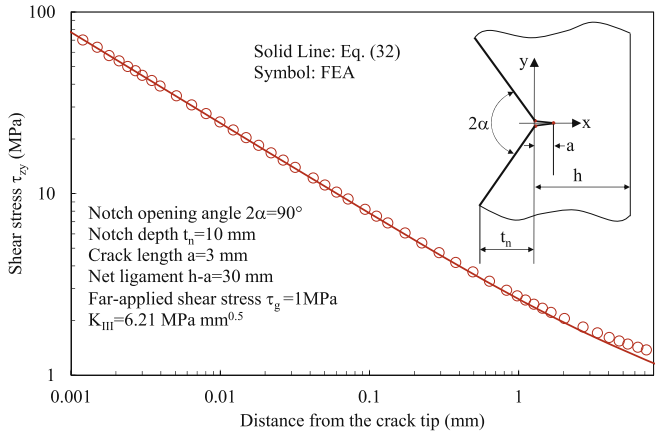

Fig. 6. Shear stress distribution along the crack line. Comparison between Eq. (32) and FE results. Finite plate with a 3 mm long crack nucleating from a pointed V notch. Uniform antiplane shear loadings.

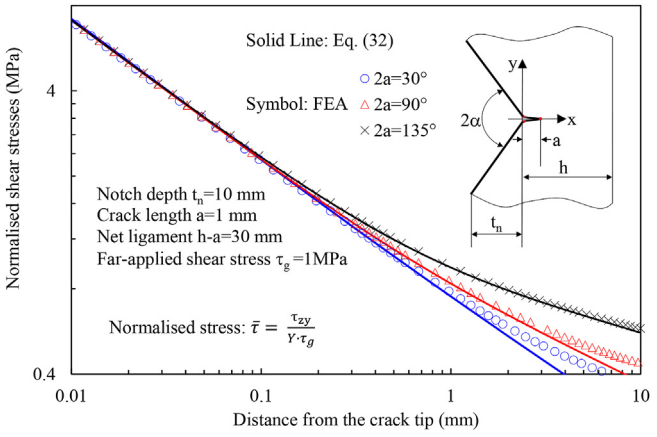

Fig. 9. Shear stress distribution along the crack line. Comparison between Eq. (32) and FE results. Finite plate with a 1 mm long crack nucleating from pointed V notches with different opening angles. Uniform antiplane shear loadings.

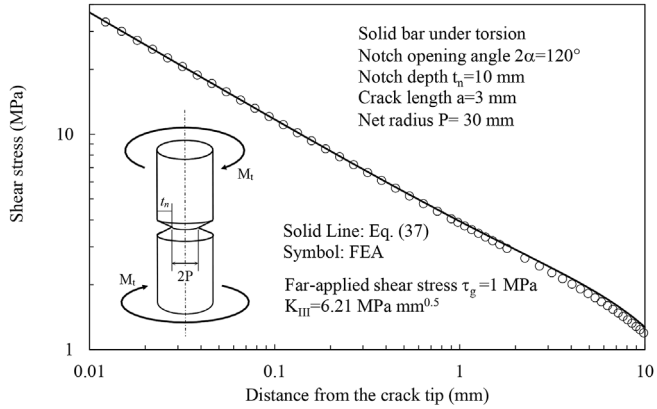

Fig. 10. Shear stress distribution along the crack line. Comparison between Eq. (37) and FE results. Finite plate with a 3 mm long crack nucleating from a pointed V notch. Solid bar under torsion.

under torsion weakened by a crack nucleated at the tip of pointed V-notches. It is evident that the accuracy of Eq. (37) is extremely satisfactory, documenting that the present solution for the stress fields can be applied also to the torsion case.

Finally, Fig. 11 shows a comparison between the dimensionless function assessed using Eq. (61), valid for cracks from shallow V notches under uniform antiplane shear loadings and the numerical results. The latter were obtained on plates with a net ligament equal to 600 mm weakened by a pointed V-notch with depth t_n = 10 mm, from which cracks of different length were thought to be nucleated. Different notch opening angles were considered, namely 2α = 30°, 90°, 120° and 135° showing, in all cases, a very satisfactory agreement. It is also evident that increasing the normalized crack length, the effect of the notch opening angle becomes less and less important.

6. Conclusions

In this work, an exact yet simple stress field solution for a crack emanating from a pointed V notch in a plate subjected to antiplane shear loading and in a solid bar under torsion was provided by combining the conformal mapping technique and a recently developed complex potential approach. Two relevant cases were addressed and solved:

- the mode III problem of a finite crack nucleating from a deep pointed V notch in a body with a finite ligament;
- the mode III problem of a finite crack nucleating from a finite depth pointed V notch in a body with an infinite ligament.

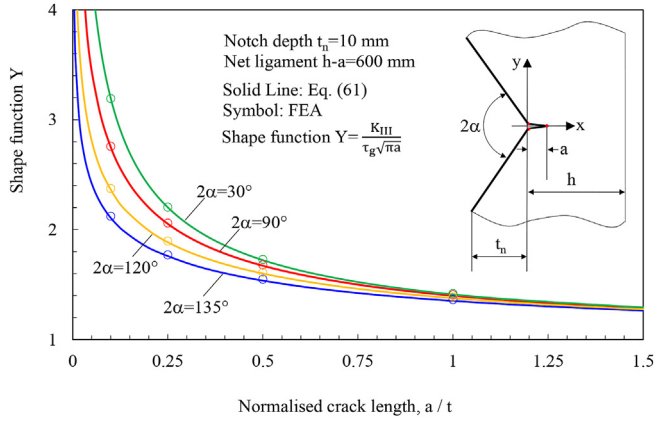

Fig. 11. Mode III shape function for cracks emanating from shallow V-notches. Comparison between Eq. (61) and FE results carried out on finite plates under uniform antiplane shear loadings. Notch depth t_n = 10 mm, net ligament h-a = 600 mm. Different notch opening angles and crack lengths.

Relevant, exact, expressions for the mode III crack stress intensity factors were provided, as well.

The accuracy of the proposed solutions was discussed taking advantage of the comparison with the results from FE analyses carried out on elastic bodies subjected to antiplane shear and torsion loadings, showing a very satisfactory agreement.

Acknowledgments

Marco Salviato acknowledges the financial support from the Haythornthwaite Foundation through the ASME Haythornthwaite Young Investigator Award and from the University of Washington Royalty Research Fund. This work was also partially supported by the William E. Boeing Department of Aeronautics and Astronautics as well as the College of Engineering at the University of Washington through Salviato's start up package.

Michele Zappalorto and Lucio Maragoni wish to acknowledge the support and the computational resources made available by the High Performance Computing Lab at the Department of Management and Engineering (DTG), co-funded by the University of Padova in the framework of the program “Scientific research instrumentation 2015”.

References

Abdelmoula, R., Semani, K., Li, J., 2007. Analysis of cracks originating at the boundary of a circular hole in an infinite plate by using a new conformal mapping approach. Appl. Math. Comput. 188, 1891–1896.
Andrews, G.E., Askey, R., Roy, R., 1999. Special Functions. Encyclopedia of Mathematics and its Applications, vol 71 Cambridge University Press.
Atzori, B., Lazzarin, P., Meneghetti, G., 2003. Fracture mechanics and notch sensitivity. Fatigue Fract. Eng. M. 26, 257–267.
Bandyopadhyay, S.N., Deysarker, H.K., 1981. Stress intensity factor for a crack emanating from the root of a semi-circular edge notch in a tension plate. Eng. Fract. Mech. 14, 373–384.
Bowie, O.L., 1956. Analysis of an infinite plate containing radial cracks originating at the boundary of an internal circular hole. J. Math. Phys. 35, 60–71.
Carraro, P.A., Maragoni, L., Quaresimin, M., 2015. Influence of manufacturing induced defects on damage initiation and propagation in carbon/epoxy NCF laminates. Adv. Manuf. Polym. Compos. Sci. 1, 44–53.
Creager, M., Paris, P.C., 1967. Elastic field equations for blunt cracks with reference to stress corrosion cracking. Int. J. Fract. Mech. 3, 247–252.
Felger, J., Becker, W., 2017. A complex potential method for the asymptotic solution of wedge problems using first-order shear deformation plate theory. Eur. J. Mech. Solid. 61, 383–392.
Ferjani, M., Averbuch, D., Constantinescu, A., 2011. A computational approach for the fatigue design of threaded connections. Int. J. Fatig. 33, 610–623.
Greenberg, M.D., 2001. Advanced Engineering Mathematics. Prentice Hall, New Jersey.
Hasebe, N., Ishida, J., 1978. A crack originating from a triangular notch on a rim of a semi-infinite plate. Eng. Fract. Mech. 10, 773–782.
Hasebe, N., Ueda, M., 1980. Crack originating from a square hole corner. Eng. Fract. Mech. 13, 913–923.
Iida, J., Hasebe, N., 2016. Stress intensity factors of a rhombic hole with symmetric cracks under uniform transverse thin plate bending. Eng. Fract. Mech. 156, 16–24.
Inglis, C.E., 1913. Stresses in a plate due to the presence of cracks and sharp corners. Trans. Inst. Nav. Archit. 55, 219–230.
Isida, M., Nakamura, Y., 1980. Edge cracks originating from an elliptical hole in a wide plate subjected to tension and in-plane shear. Trans. Jpn. Soc. Mech. Engrs. 46, 947–956.
Jones, R., Peng, D., 2002. Simple method for computing the stress intensity factors for cracks at notches. Eng. Fail. Anal. 9, 683–702.
Kujawski, D., 1991. Estimations of stress intensity factors for small cracks at notches. Fatigue Fract. Eng. M. 14, 953–965.
Kullmer, G., 1992. Elastic stress fields in the vicinity of a narrow notch with circular root. Reliability and structural integrity of advanced materials. In: Proceedings of the 9th Biennial European Conference on Fracture (ECF 9), vol. II. pp. 905–910 Varna, Bulgaria.
Lazzarin, L., Tovo, R., 1996. A unified approach to the evaluation of linear elastic stress fields in the neighborhood of cracks and notches. Int. J. Fract. 78, 3–19.
Lazzarin, P., Tovo, R., Meneghetti, G., 1997. Fatigue crack initiation and propagation phases near notches in metals with low notch sensitivity. Int. J. Fatig. 19, 647–657.
Levenberg, K., 1944. A method for the solution of certain non-linear problems in least squares. Q. Appl. Math. 2, 164–168.
Livieri, P., Lazzarin, P., 2005. Fatigue strength of steel and aluminium welded joints based on generalised stress intensity factors and local strain energy values. Int. J.

Fract. 133, 247–276.
Lukas, P., Klesnil, M., 1978. Fatigue limit of notched bodies. Mater. Sci. Eng. 34, 61–66.
Maragoni, L., Carraro, P.A., Quaresimin, M., 2016. Effect of voids on the crack formation in a [45/-45/0](s) laminate under cyclic axial tension. Compos Part A-Appl S 91, 493–500.
Marquardt, D., 1963. An algorithm for least-squares estimation of nonlinear parameters. SIAM J. Appl. Math. 11, 431–441.
Muki, R., Westmann, R.A., 1974. Crack emanating from an open notch. J. Elasticity 4, 173–186.
Murakami, Y., 1978. A method of stress intensity factor calculation for the crack emanating from an arbitrarily shaped hole or the crack in the vicinity of an arbitrarily shape hole. Trans. Jpn. Soc. Mech. Eng. 44, 423–432.
Neal, D.M., 1970. Stress Intensity Factors for cracks emanating from rectangular cutouts. Int. J. Fract. Mech. 6, 393–400.
Neuber, H., 1958. Theory of Notch Stresses: Principles for Exact Calculation of Strength with Reference to Structural Form and Material. Springer-Verlag, Berlin.
Newman Jr., J.C., 1971. An improved method of collocation for the stress analysis of cracked plates with various shaped boundaries. NASA TN D-6376 1–45.
Philipps, A.G., Karuppanan, S., Churchman, C.M., Hills, D.A., 2008. Crack tip stress intensity factors for a crack emanating from a sharp notch. Eng. Fract. Mech. 75, 5134–5139.
Salviato, M., Zappalorto, M., 2016. A unified solution approach for a large variety of antiplane shear and torsion notch problems: theory and examples. Int. J. Solid Struct. 102–103, 10–20.
Schijve, J., 1982. The stress intensity factor of small cracks at notches. Fatigue Fract. Eng. M. 5, 77–90.
Sokolnikoff, I.S., 1983. Mathematical Theory of Elasticity. Krieger Pub Co.
The, L.S., Love, A.J., Brennan, F.P., 2006. Mode I stress intensity factors for edge cracks emanating from 2-D U-notches using composition of SIF weight functions. Int. J. Fatig. 28, 355–365.
Timoshenko, S.P., Goodier, J.N., 1970. Theory of Elasticity, third ed. McGraw-Hill, New York.
Tweed, J., Rooke, D.P., 1973. The distribution of stress near the tip of a radial crack at the edge of a circular hole. Int. J. Eng. Sci. 11, 1185–1195.
Weißgraeber, P., Felger, J., Geipel, D., Becker, W., 2016a. Cracks at elliptical holes: stress intensity factor and Finite Fracture Mechanics solution. Eur. J. Mech. Solid. 55, 192–198.
Weißgraeber, P., Leguillon, D., Becker, W., 2016b. A review of Finite Fracture Mechanics: crack initiation at singular and non-singular stress raisers. Arch. Appl. Mech. 86, 375–401.
Xu, R.X., Topper, T.H., Thompson, J.C., 1997. Mode I stress intensity factor equations for cracks at notches and cavities. Fatigue Fract. Eng. M. 20, 1351–1361.
Yan, X., 2004. Analysis for a crack emanating from a corner of a square hole in an infinite plate using the hybrid displacement discontinuity method. Appl. Math. Model. 28, 835–847.
Yan, X., 2005. Stress intensity factors for cracks emanating from a triangular or square hole in an infinite plate by boundary elements. Eng. Fail. Anal. 12, 362–375.
Yan, X., 2006. Cracks emanating from circular hole or square hole in rectangular plate in tension. Eng. Fract. Mech. 73, 1743–1754.
Yoshida, M., 1997. Hypergeometric Functions, My Love: Modular Interpretations of Configuration Spaces. Friedr. Vieweg & Sohn, Braunschweig – Wiesbaden.
Yosibash, Z., Mittelman, B., 2016. A 3-D failure initiation criterion from a sharp V-notch edge in elastic brittle structures. Eur. J. Mech. Solid. 60, 70–94.
Zappalorto, M., Lazzarin, P., 2011. In-plane and out-of-plane stress field solutions for V-notches with end holes. Int. J. Fract. 168, 167–180.
Zappalorto, M., Lazzarin, P., Filippi, S., 2010. Stress field equations for U and blunt V-shaped notches in axisymmetric shafts under torsion. Int. J. Fract. 164, 253–269.
Zappalorto, M., Maragoni, L., 2018. Nonlinear mode III crack stress fields for materials obeying a modified Ramberg-Osgood law. Fatigue Fract. Eng. M. 41, 708–714.